OPEN ACCESS

UNIVERSITY OF DUNDEE

University of Dundee

Static and cyclic rocking on sand

Kokkali, P.; Anastasopoulos, I.; Abdoun, T.; Gazetas, G.

Link to publication in Discovery Research Portal

Static and cyclic rocking on sand: centrifuge versus reduced-scale 1*g* experiments

P. KOKKALI*, I. ANASTASOPOULOS†, T. ABDOUN* and G. GAZETAS‡

Shallow foundations supporting bridge piers, building frames, shear walls and monuments are often subjected to extreme lateral loading such as wind in offshore environments, or strong seismic shaking. Under such loading conditions, foundations may experience a host of non-linear phenomena: sliding on and uplifting from the supporting soil or even soil failure in the form of development of ultimate bearing capacity mechanisms. This type of response is accompanied by residual settlement and rotation of the supported structural system. Nevertheless, inelastic foundation performance can provide potential benefits to the overall seismic integrity of the structure. Thanks to such non-linearities, energy dissipation at or below the foundation level may eventually limit the seismic demand on structural elements. Several theoretical and experimental studies have provided encouraging evidence to this effect. This paper has a dual objective: first, to study the behaviour of shallow foundations under vertical and lateral monotonic loading and under lateral slow cyclic loading of progressively increasing amplitude; second, to explore the differences in foundation response between reduced-scale 1*g* and centrifuge 50*g* model testing. Emphasis is placed on interpreting their discrepancies by unveiling the role of scale effects. The role of soil densification due to multiple loading cycles with uplifting is also highlighted.

KEYWORDS: bearing capacity; centrifuge modelling; footings/foundations; settlement

INTRODUCTION

The importance of non-linear soil–foundation–structure inter-action under lateral loading has been acknowledged by the engineering community, especially for offshore structures which are typically subjected to multicycle wind and wave loading. In the case of seismic shaking, with the recorded acceleration levels by far exceeding the conventional design guidelines in recent seismic events, it has become evident that inelastic foundation response is often unavoidable. Shallow foundations supporting bridge piers or building columns and shear walls may experience sliding and/or uplifting from the supporting soil, or bearing capacity failure in softer soils. Usually, such non-linear response is accompanied by permanent settlement and/or rotation. However, such mobilisation of strongly inelastic response also reduces the seismic demand and may therefore be beneficial for the seismic performance of the structural system. The potential benefits from these types of non-linearity have been indicated by several researchers (Priestley *et al.*, 1996; Pecker & Pender, 2000; Gazetas & Apostolou, 2004; Mergos & Kawashima, 2005; Gajan & Kutter, 2008; Anastasopoulos *et al.*, 2010a; Gelagoti *et al.*, 2012; Kourkoulis *et al.*, 2012).

Several studies have explored the behaviour of foundations under lateral and combined loading, both theoretically (Nova & Montrasio, 1991; Butterfield & Gottardi, 1994; Paolucci, 1997; Bransby & Randolph, 1998; Martin & Houlsby, 2001; Gourvenec & Randolph, 2003; Chatzigogos *et al.*, 2009) and experimentally (Negro *et al.*, 2000; Gajan *et al.*, 2005; Gajan & Kutter, 2008; Paolucci *et al.*, 2008; Anastasopoulos *et al.*,

2012, 2013; Deng *et al.*, 2012; Drosos *et al.*, 2012). Experimental studies have significantly contributed to the understanding of the rocking response of shallow foundations. Nevertheless, many of them have been conducted at a low confining stress environment (reduced-scale 1*g* testing). Compared to centrifuge model testing, 1*g* experiments are easier and more economical to perform but cannot reproduce the actual stress field in the soil. Owing to the low prevailing confining stresses in 1*g* test conditions, the angle of shearing resistance and the small strain stiffness of the soil are typically much larger compared to realistic stress levels. Such issues may have a substantial effect on the measured response and therefore 1*g* tests should be carefully designed and the results should be interpreted accordingly.

In an attempt to clarify these issues, commonly referred to as 'scale effects', a qualitative and quantitative comparison of the rocking response of shallow foundations obtained from centrifuge and reduced-scale 1*g* experiments is presented in this paper. Simple slender systems founded on dry sand are designed to be equivalent in terms of vertical factor of safety. They are then subjected to lateral monotonic loading till overturning and lateral slow cyclic loading. The response of the equivalent systems is compared in terms of moment capacity, settlement accumulation during cyclic loading, stiffness degradation and energy dissipation. The results elucidate some salient features of the behaviour of shallow foundations subjected to large deformations, offering a quantification of the role of scale effects in cyclic foundation response.

PROBLEM DEFINITION AND EXPERIMENTAL METHODOLOGY

A series of centrifuge model tests were conducted in the 3 m radius, 150 g-tonne capacity centrifuge of the Centre for Earthquake Engineering Simulation at Rensselaer Polytechnic Institute (RPI). The corresponding reduced-scale 1*g* tests were performed at the Laboratory of Soil Mechanics of the

National Technical University of Athens (NTUA). The experimental investigation focuses on the response of a rigid single mass slender system supported on a surface footing and subjected to monotonic and slow cyclic lateral loading. The prototype soil–structure system studied is shown in Fig. 1(a). Founded on a square surface footing of width $B = 3$ m, the system has its centre of mass located at 6·9 m above ground. The oscillator is rigid in order to focus on the non-linear foundation response. The supporting soil consists of dry sand of adequate thickness $D \approx 3 \cdot 3B$ ($= 10$ m), con-

Fig. 1. Schematic illustration of the soil–structure systems studied: (a) prototype system; (b) centrifuge model; (c) reduced-scale 1*g* model

sidering the shallow nature of the rocking failure mechanism.

This prototype system was appropriately scaled down according to the relevant centrifuge and 1*g* scaling laws (Wood, 2003) and the resulting geometries for the centrifuge and the 1*g* models are shown in Fig. 1. The lateral loading tests were conducted at a 50*g* centrifuge acceleration (1:50 scale) and a scale of 1:20 was selected for the reduced-scale 1*g* tests. Vertical push tests were conducted prior to the lateral push tests in order to determine the bearing capacity of the soil–foundation systems and the corresponding vertical factors of safety (F_S). The experimental configurations for the centrifuge and the 1*g* tests are presented in the following paragraphs and details about the modelling and the critical design parameters are also provided.

Experimental set-up for centrifuge tests

The experimental configurations for the vertical and lateral loading centrifuge tests are depicted in Fig. 2. A four-degrees-of-freedom in-flight robot designed to perform multiple tasks while the centrifuge is spinning was used in the experimental series. The robot is capable of articulating in three linear dimensions and rotating around one axis with variable speed. It can operate in single instruction mode or follow programmatic scripts. Custom tools for the end of the robotic arm (robot end-effector) were fabricated for the vertical and lateral push tests. While the bearing capacity tests and the lateral monotonic push-over tests were conducted in manual mode, the robot was programmed for the application of the cyclic loading path assuring control and consistency of the applied displacement and velocity through all the loading cycles.

The set-up for the vertical push tests is shown in detail in Fig. 2(a) (plan view) and Fig. 2(b) (side view). A model square steel foundation of width B connected to the robot custom tool was placed at the centre of a square container. Adequate distance from the lateral boundaries (5B) was assured so that boundary effects were avoided. The foundation was pushed down until bearing capacity failure was indicated. The vertical displacement was applied and recorded by the robot and the reaction load was measured by the robot load cell.

A rectangular container provided two test locations for the monotonic and the slow cyclic lateral push tests. Adequate distance from the box lateral boundaries (4B) and between the two test locations (5B) was assured to minimise boundary effects and interference between the different tests (Figs 2(c) and 2(d)). The structure was a three-piece unit comprising a steel foundation, a steel column and a steel mass located at a specified height. Sandpaper was placed beneath the foundation in order to attain an adequately rough foundation–soil interface and minimise sliding. A spherical aluminium attachment on top of the structure was pushed laterally by the robot during cyclic loading. This structure–sphere assembly was properly designed so that the structure could freely move without any lateral or vertical restraints. Details of this connection are shown in Fig. 2(d) and later in Fig. 4(c). After cyclic testing, the structure was moved to the second test location for the monotonic push-over test, and lateral displacement was applied against the side face of the structure until it overturned.

A biaxial load cell, connected to the robot custom tool, measured the horizontal force in both the loading (x) and the transverse (y) direction, while the vertical force was monitored by the robot load cell. On-board cameras captured the horizontal and vertical displacements and rotation of the structure. Specialised software was used to analyse the recorded videos and extract displacement–time histories.
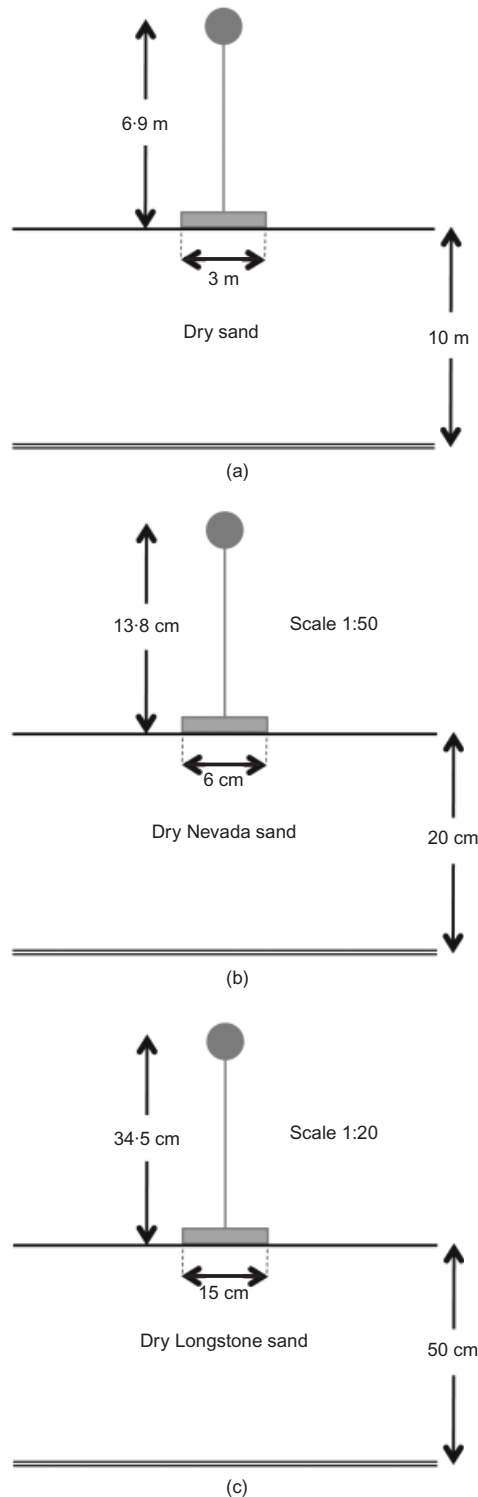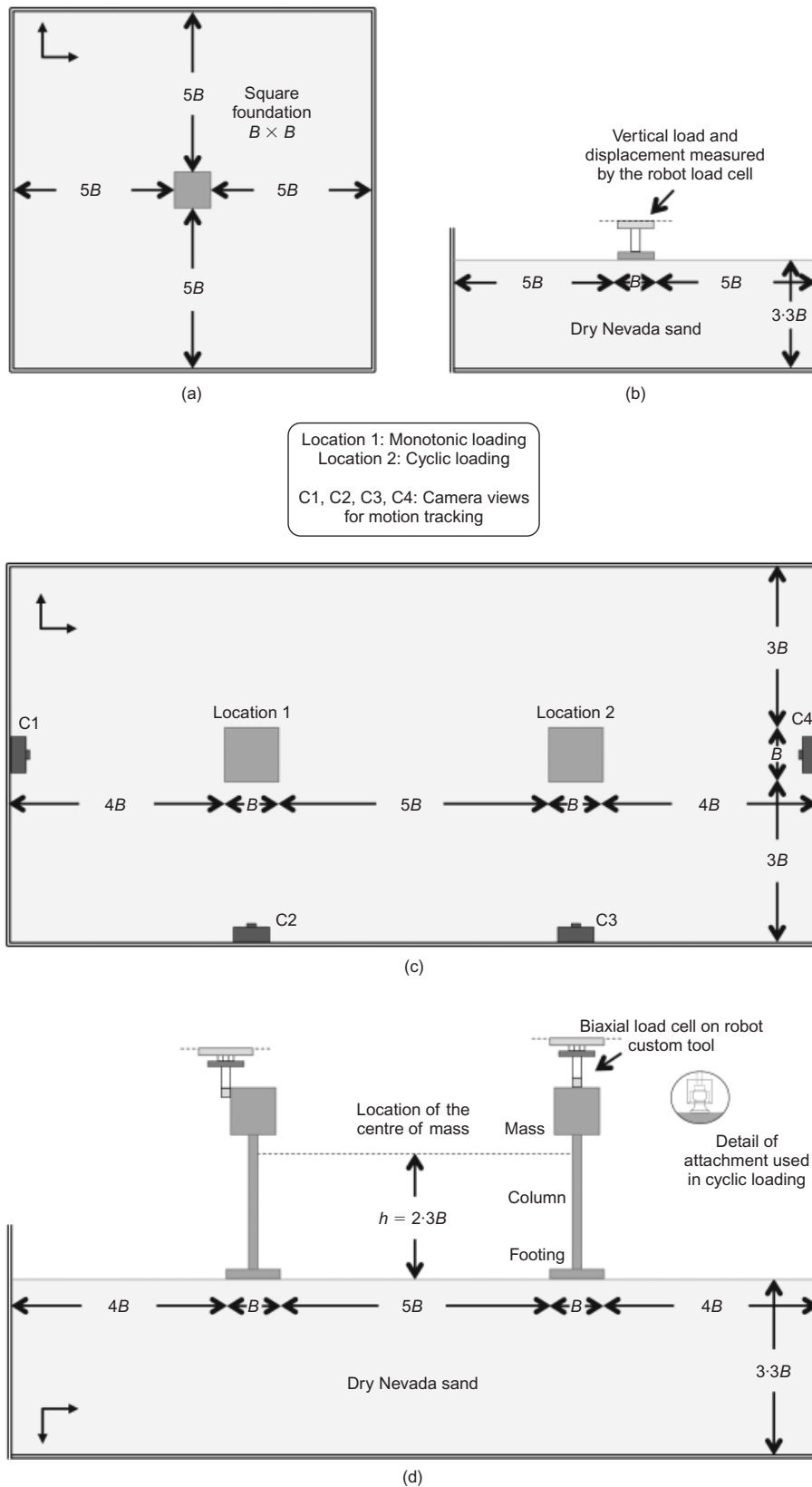
Fig. 2. Centrifuge model containers and experimental set-up for vertical and lateral loading tests: (a) vertical push test: plan view; (b) vertical push test: side view; (c) lateral push test: plan view; and (d) lateral push test: side view along the loading axis

Tracking targets were mounted on the structure along each axis, and high-intensity light-emitting diodes (LEDs), placed at appropriate angles to minimise glare and reflection, enhanced video quality thus facilitating motion tracking. After the cameras and the structure were placed at their final locations, the cameras focused on a square grid in order to correct for lens distortion and field of view perpendicularity. The corrected video was then loaded into the software package Tema for tracking. Fig. 3 shows a snapshot during tracking of a lateral monotonic push-over test.
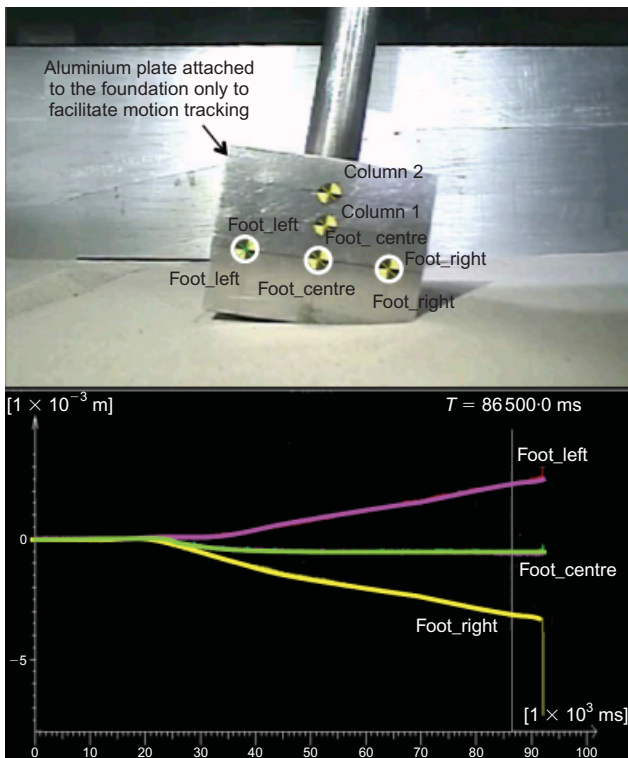
Fig. 3. Motion tracking during monotonic push-over test (snapshot from Tema software)

An important part of the set-up procedure of the lateral push tests was the surface preparation and the alignment of the structure with respect to the robot loading axis. Placing the foundation with an initial inclination in any direction could result in undesired pre-stressing of the soil or biaxial loading. Therefore, the soil surface was levelled and the structure was precisely aligned to the robot loading axis, as shown in Fig. 4. In both cases, the robot custom tools were utilised to smooth and level the soil surface without disturbing the soil density and to place the footing at the specified test location. Fig. 4(c) shows the structure placed at the cyclic loading test location and the camera view used to track the motion of the footing along the loading axis.
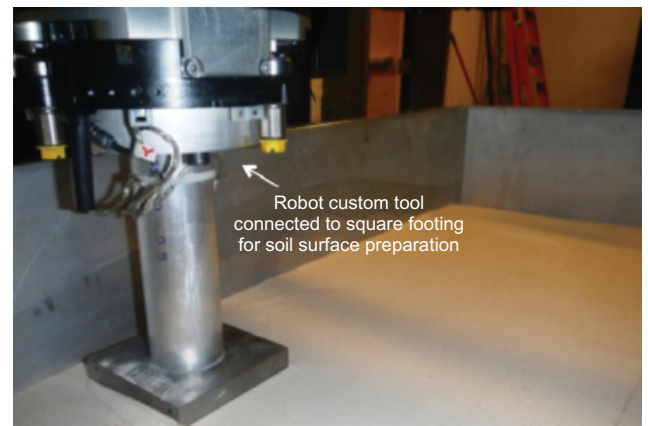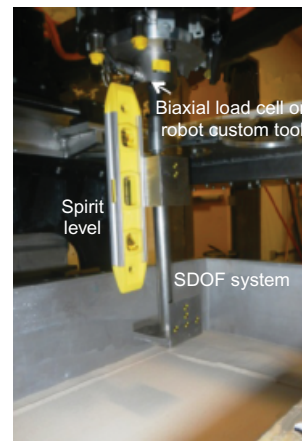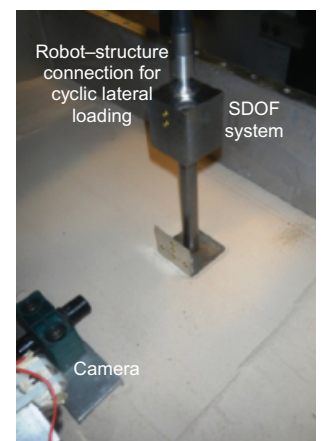
Fig. 4. Centrifuge lateral push tests: (a) soil surface preparation; (b) alignment and placement of structure on soil surface; (c) structure located at test location

Experimental set-up for reduced-scale 1g tests

Similar experimental configurations were developed in the reduced-scale 1*g* test series. Fig. 5(a) shows the set-up of the bearing capacity tests and Fig. 5(b) the one used in the lateral push tests. The locations of the models with respect to the lateral boundaries of the rigid container used in the
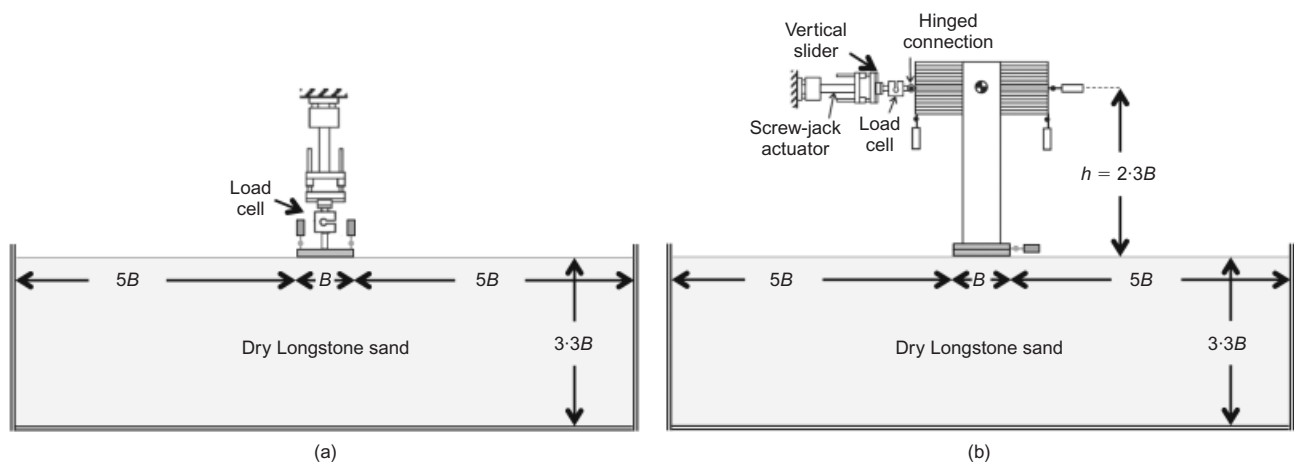
Fig. 5. Model containers and experimental set-up for reduced-scale 1g tests: (a) vertical push test set-up; (b) lateral push test set-up

experimental series are also shown. A push-over apparatus, fixed to a reaction wall and consisting of a servomotor attached to a screw-jack actuator, was used to apply the vertical or horizontal displacement. Four laser displacement transducers measured the settlement of the four corners of the footing during the vertical test and a load cell connected to the edge of the actuator measured the vertical reaction force.

The foundation–structure model consisted of a square aluminium footing rigidly connected to a pair of rigid steel columns that supported an aluminium slab. Steel plates were symmetrically placed above and below the slab to model the system's mass. Sandpaper was used beneath the foundation to simulate a realistically rough soil–footing interface. In this set-up the free end of the actuator was connected to the structure model using a vertical slider and a hinged connection in series. This connection allowed the system to freely settle, slide or rotate as horizontal displacement was applied. The horizontal load was measured by a load cell inserted between the vertical slider and the hinged connection. Horizontal and vertical displacements were recorded through a system of wire and laser displacement transducers. Accurate positioning of the structure at the test location without disturbing the soil surface was achieved by a system of four mechanical jacks. Photographs of the experimental configuration are shown in Fig. 6.

Soil properties and samples preparation

Nevada 120 sand was dry pluviated to the desired density with a consistent manual technique in the centrifuge test series. Dry Longstone sand was layered in the 1g test container through an electronically controlled raining system, capable of producing sand specimens of controllable relative density. The raining system has been calibrated through a series of pluviation tests documented in Anastasopoulos *et al.* (2010b). Nevada 120 sand is a laboratory grade with $D_{50} = 0\cdot15$ mm and uniformity coefficient $C_u = 2\cdot35$. Longstone sand is an industrially produced fine and uniform quartz sand, also having $D_{50} = 0\cdot15$ mm and uniformity coefficient $C_u = 1\cdot42$. The grain size distribution of both sand specimens is shown in Fig. 7 and their properties are summarised in Table 1.

The stress level prevailing in the 1g tests is unavoidably low; therefore, the strength characteristics of Longstone sand need to be known at a wide range of stresses. Fig. 8 shows the dependence of the angle of shearing resistance ϕ on the normal stress level, as described in Anastasopoulos *et al.* (2010b) based on laboratory tests performed for two relative densities ($D_r = 45\%$ and 80%). The friction angle of Nevada sand at three relative densities ($D_r = 40\%$, 60% and 70%), at a reference mean effective normal stress $\sigma = 100$ kPa, is also shown as three points in Fig. 8 (Arulmoli *et al.*, 1992). The two stress ranges prevailing at a depth equal to one foundation width in each type of test are also depicted. The lower bound corresponds to the average geostatic stress for these densities at this reference depth. The upper bound takes into account the dead load of the superstructure. This diagram will be revisited in the discussion of the test results later on.

Superstructure modelling

Instead of scaling the dead load of the superstructure, a different methodology was followed, namely the vertical load over capacity ratio of the compared systems was kept constant in each set of experiments. This ratio is expressed through the vertical factor of safety F_S and is directly correlated to the rocking response of shallow
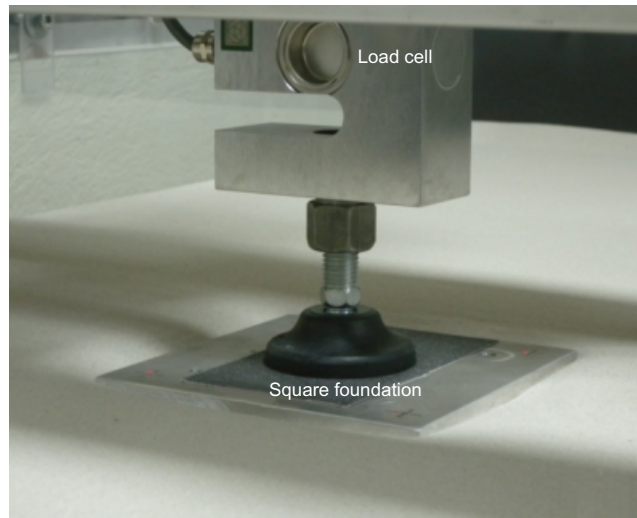
(a)
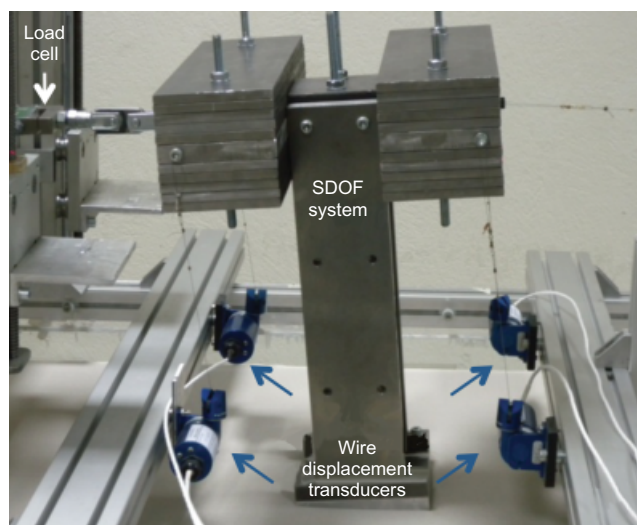
(b)

Fig. 6. Photographs of the reduced-scale 1g tests: (a) vertical push test; (b) cyclic lateral push test
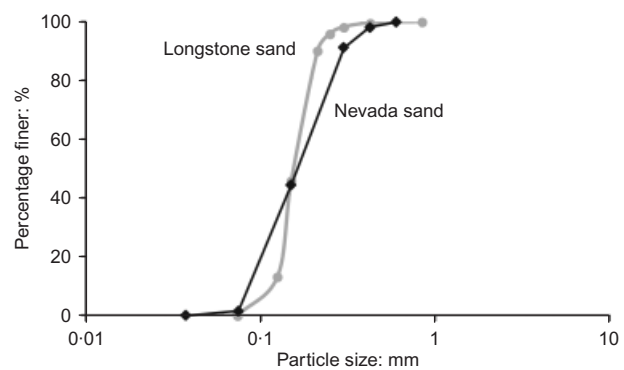

Fig. 7. Grain size distribution of Nevada and Longstone sand

Table 1. Summary of soil properties for Nevada and Longstone sand

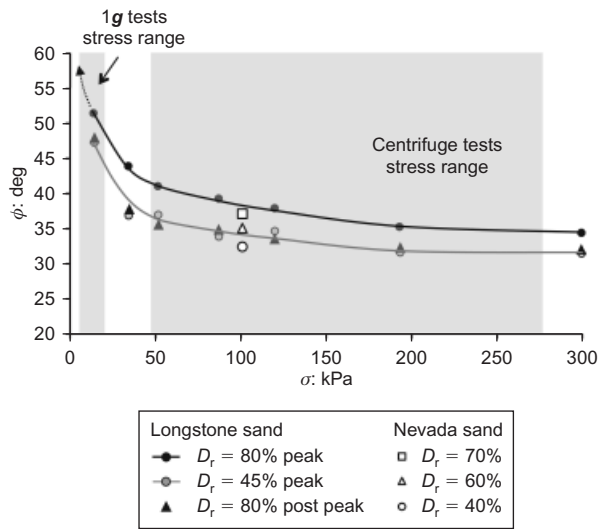| Properties	Nevada 120 sand	Longstone sand
e_{max}	0·887	0·995
e_{min}	0·511	0·614
D_{50}	0·15 mm	0·15 mm
C_u	2·35	1·42
G_s	2·67	2·64

Fig. 8. Direct shear test results for Longstone sand: dependence of the angle of shearing resistance on stress level (Anastasopoulos *et al.*, 2010b). Friction angle for Nevada sand: evaluation from isotropically consolidated undrained compression tests at reference mean effective normal stress 100 kPa (Arulmoli *et al.*, 1992). The stress ranges at a depth equal to one foundation width are also depicted. The lower bound corresponds to the geostatic stress at this depth. The upper bound includes the geostatic stress and the stress induced by the structure dead weight

foundations, distinguishing the sinking from the uplifting rocking response. Additionally, the location of the centre of mass is a crucial design parameter related to the geometric non-linearity of the system through the slenderness ratio h/B, which controls the uplifting and overturning potential as well as the ultimate moment capacity of the foundation.

According to the above, the mass and geometry of the structure models were designed so that the equivalent centrifuge and $1g$ single degree of freedom (SDOF) systems had the same F_S and $h/B = 2\cdot3$. In terms of the vertical factor of safety F_S, the bearing capacity tests provided the ultimate vertical load of each soil–footing system and the mass of the superstructure was then adjusted to satisfy the F_S criterion. As already mentioned, no attempt was made to model the flexibility of the superstructure and both models were sufficiently rigid so that the system's response was governed by non-linear soil–foundation response.

BEARING CAPACITY TESTS

Two uniform soil profiles were considered: a loose sand of relative density $D_r = 45\%$ and a very dense sand of $D_r = 90\%$. Two-layer soil profiles were also tested, consisting of a loose ($D_r \approx 45\%$) bottom layer and a dense ($D_r \approx 90\%$) upper layer depth z. In the following, the depth of the upper dense layer (z) is normalised by the foundation width: z/B. Two layered profiles were investigated: $z/B = 0\cdot25$ and $0\cdot5$. The model square foundations were subjected to vertical push tests in order to estimate the bearing capacity of four soil–foundation systems and design the centrifuge and the $1g$ superstructures. In the following paragraphs, a comparison between the two types of tests is presented. All results correspond to prototype units.

Figure 9 compares the vertical load–settlement curves of each of the four soil profiles. A first comparison reveals discrepancies between the centrifuge and the $1g$ response. The $1g$ models sustain higher vertical loads than the corresponding centrifuge systems. The significantly steeper initial slopes of the $1g$ load–settlement curves indicate a larger

vertical stiffness of the $1g$ soil–foundation systems. Despite these differences, some interesting common trends can be observed: while the capacity of the foundation on dense sand eventually reaches a constant value (plateau of the curve), a continuing increase of the vertical load is observed for the loose and the two-layer soil profiles. This 'hardening' behaviour can be attributed to the stiffening of the loose supporting soil as the footing is pushed into the ground, in combination with the contribution of the footing embedment to the bearing capacity (for all four configurations). The vertical load capacity N_u of each system is also shown in Fig. 9. These values were determined in a consistent way for all eight tests. For the tests on loose sand and on the two-layer profiles the definition of the ultimate load is not straightforward because of the hardening behaviour. In this study, N_u was defined as the load for which the rate of change of the vertical stiffness became constant. In addition, the choice of the N_u point was consistent when comparing the same profiles at $1g$ and high g level.

A summary of the vertical load capacities as well as the ratio of the $1g$ to the centrifuge ultimate loads is provided in Table 2. The $1g$ vertical load capacities are 30–70% higher than the loads sustained in the centrifuge tests. The differences observed between the two sets of tests can be further explored in view of the scale effects affecting the $1g$ foundation response. Nevada and Longstone sands exhibit comparable shear resistance at large stress levels and similar densities, as evidenced in Fig. 8. Nevertheless, below 50 kPa confining pressure the shearing resistance of Longstone sand exhibits a remarkable increase. As shown in the figure, the stress level for the $1g$ tests falls in this range, hence the overestimation of the friction angle and thereby of the ultimate vertical loads. To further verify this response, the classical expression of Meyerhof (1951) for the bearing capacity of a surface rectangular footing was employed to back-calculate the effective friction angle of the dense and loose soil profiles. Whereas for the centrifuge tests the friction angle of the loose and the dense sand was calculated to be $33\cdot5°$ and $38\cdot5°$, respectively, the friction angles of the same profiles at $1g$ were $47°$ and $50°$.

Interestingly, the deviation between the centrifuge and the $1g$ load–settlement curves becomes more considerable for the dense soil (Table 2), indicating that the overestimation of the friction angle is more prominent for a dense sand profile with distinct dilative behaviour. Regarding the two-layer profiles, the response is affected by both soil layers. Revisiting Fig. 9, it can be noticed that the behaviour resembles the response of the underlying loose sand, which is of dominant importance in this deep failure mechanism.

ROCKING RESPONSE IN VIEW OF SCALE EFFECTS

As described above, an alternative methodology was followed for the superstructure design in order to maintain similitude by keeping the vertical factor of safety and the slenderness ratio of the models constant and directly comparing the centrifuge and the $1g$ rocking response. Thus, the loose soil profile was chosen as a reference case and the superstructure mass was adjusted and distributed so that a slenderness ratio $h/B = 2\cdot3$ and a factor of safety $F_S = 5$ were achieved for each system on loose sand. Using the same superstructures, the two-layer soil–foundation systems yielded factors of safety equal to $5\cdot5$ (for $z/B = 0\cdot25$) and 7 (for $z/B = 0\cdot5$). The factors of safety on dense sand were slightly different and in order to avoid misinterpretations of the test results this case is not be presented here. A summary of the vertical factors of safety is included in Table 2.
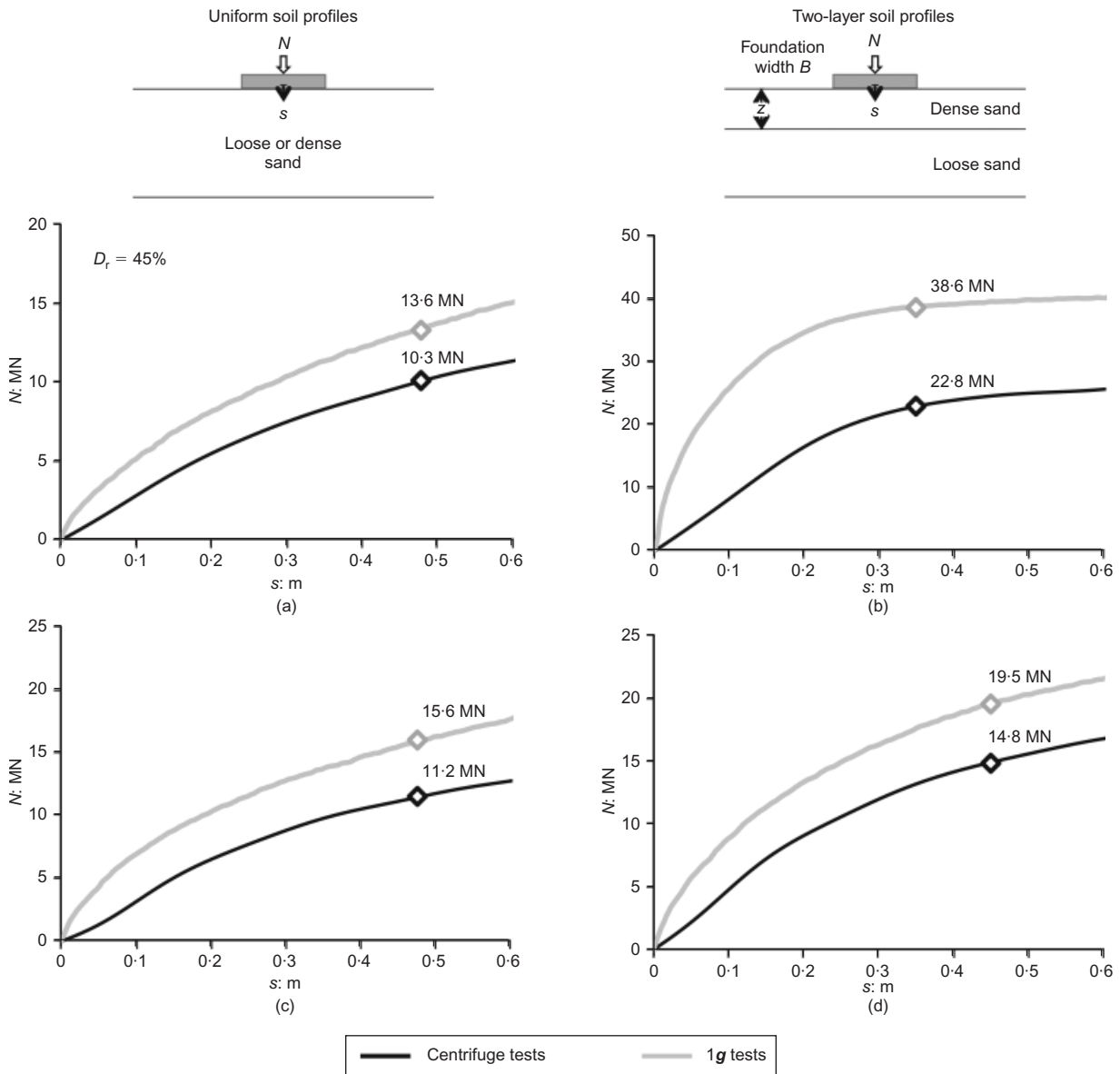
Fig. 9. Load–settlement curves obtained from monotonic vertical centrifuge and 1g push tests on four soil profiles: (a) loose sand; (b) dense sand; (c) $z/B = 0.25$; (d) $z/B = 0.5$

Table 2. Summary of vertical push-down test results

Soil profile	Centrifuge test, N_u: MN	1g test, N_u: MN	F_S		$N_{u, 1g}/N_{u \text{ centrifuge}}$
			Centrifuge model	1g model	
Loose sand	10·3	13·6	5	5	1·32
Dense sand	22·8	38·6	11	14	1·69
$z/B = 0.25$	11·2	15·6	5·5	5·5	1·39
$z/B = 0.5$	14·8	19·5	7	7	1·32

Monotonic lateral loading

The soil–structure systems described above were subjected to lateral loading until they overturned. Fig. 10 depicts the moment, the settlement and the rotational stiffness of the six systems as functions of the footing rotation. The moment is calculated as the product Fh, using the horizontal force F measured by the load cell multiplied by the lever arm h. The settlement that is induced only by the lateral loading refers to the centre of the footing. Overall, the two sets of tests show several differences between them, with the 1g

systems reaching higher moment capacities and exhibiting a more pronounced uplifting behaviour than those in the centrifuge. These trends are hardly surprising

(a) higher angle of shearing resistance results in higher moment capacity
(b) the geometric non-linearity (uplifting) in such systems is governed by the stiffness of the soil; the stiffer soil in the 1g test leads to greater uplifting.

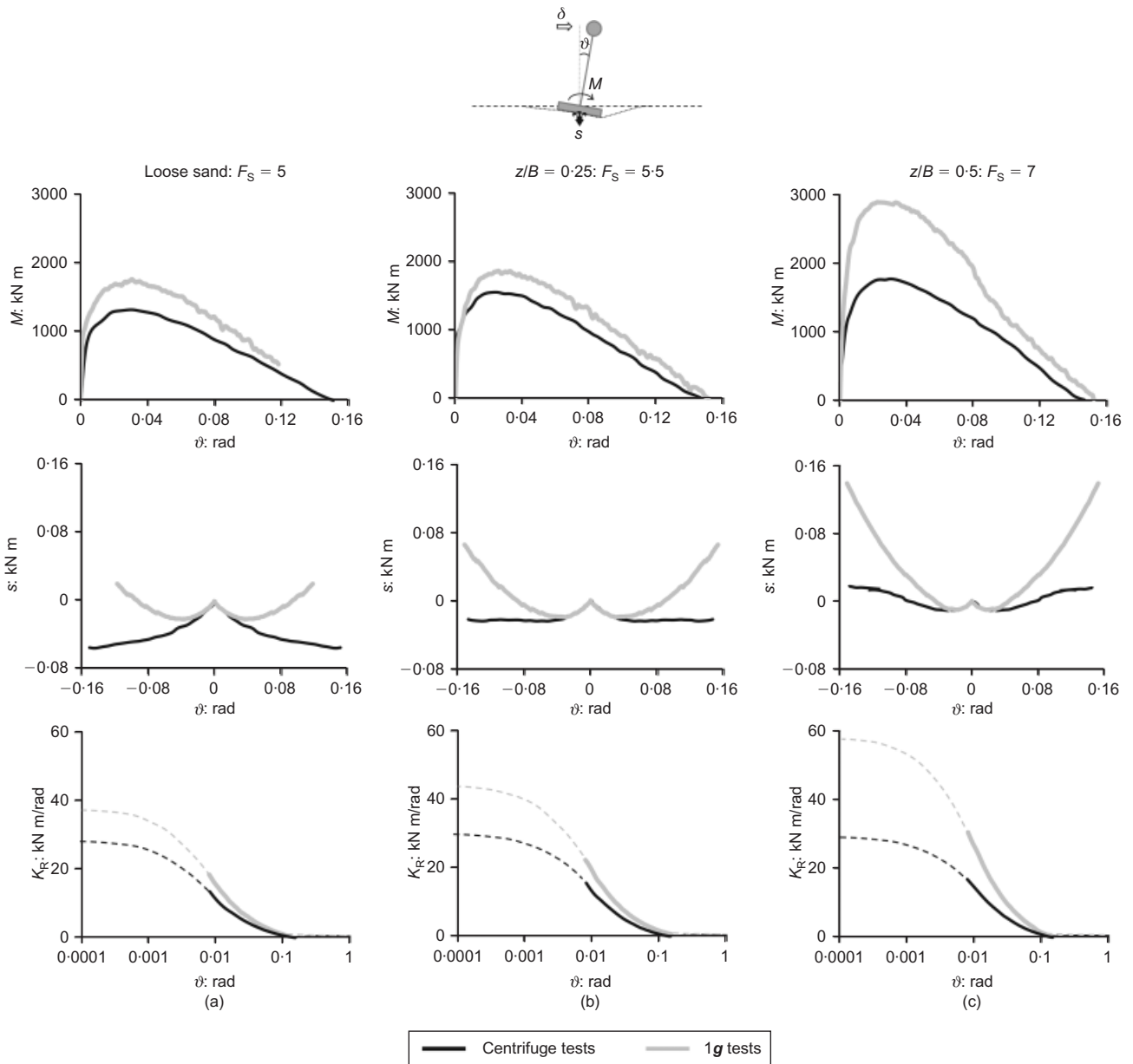When it comes to the inelastic response of the systems,

Fig. 10. Comparison of monotonic centrifuge and 1g push tests in terms of moment–rotation, settlement–rotation and rotational stiffness against rotation: (a) loose sand; (b) two-layer soil profile $z/B = 0.25$; (c) two-layer soil profile $z/B = 0.5$

that is, the moment degradation and the subsequent overturn due to P–δ effects, a very good agreement is observed in terms of the overturning angle since the systems share the same slenderness ratio.

Unsurprisingly, the moment capacity reached in the 1g two-layer system of $z/B = 0.5$ is overestimated to a greater extent than in the other two soil profiles. Since the rocking failure only extends to a very limited depth beneath the foundation, not more than half the width, it seems that scale effects become more adverse with the presence of the dilative dense upper layer that contains the rotational failure surface. The shape of the 1g moment–rotation curve reflects this behaviour. At low rotational amplitudes and therefore relatively low confining stresses, the 1g moment–rotation curve significantly deviates from the centrifuge curve. After the peak of the curve and when the stresses induced to the soil due to lateral loading have increased (around $\theta = 0.1$ rad) the 1g moment–rotation curve starts approaching the centrifuge curve and they eventually converge.

The settlement–rotation curves of the two test systems almost coincide at small rotational amplitudes while distinct differences are noticed at larger rotations. The 1g systems uplift from the supporting soil relatively quickly (uplift is denoted by the upward change of the slope of the settlement–rotation curve), whereas the centrifuge systems keep sinking (for loose sand and $z/B = 0.25$) or uplift slightly and much later (for $z/B = 0.5$). Evidently the vertical stiffness of the 1g systems is larger, following the larger soil stiffness and friction angle. The comparison under monotonic loading is concluded with the plots of the secant rotational stiffness as a function of the angle of rotation. The accurate measurement of K_R is not feasible at small rotations due to limitations in sensor accuracy. The real data are plotted for rotational amplitudes larger than 0.008 rad and curve fitting is adopted to extrapolate the small-strain rotational stiffness (dotted lines). Invariably, all the 1g systems exhibit significantly higher rotational stiffness. The deviation becomes smaller at larger rotational

amplitudes where the systems have uplifted from the supporting soil and reduction of the effective contact area has occurred. At that point, the geometric non-linearity dominates the response and the rotational stiffness quickly degrades in all cases.

Cyclic lateral loading

The performance of the SDOF systems when subjected to slow cyclic lateral loading is evaluated in this section. Gajan *et al.* (2005) have shown through a series of centrifuge tests that the response of a rocking foundation to seismic shaking can be fairly well predicted from slow cyclic tests. Fourteen cycles of increasing displacement amplitude were applied at the centre of mass of the structures (Fig. 11). The lateral displacement is normalised to the overturning displacement of the equivalent rigid block on rigid base ($\delta_R = B/2 = 1.5$ m). Even though the chosen load sequence is not representative of a specific earthquake, it allows the systems' performance to be compared under a wide range of displacement amplitudes, stressing them from their elastic all the way into their metaplastic regime.
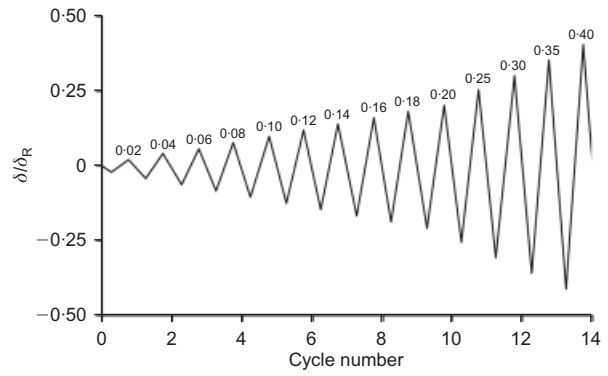

Fig. 11. Normalised cyclic lateral displacement applied at the centre of mass of SDOF systems

The cyclic response of the compared systems is outlined in terms of moment–rotation and settlement–rotation in Figs 12–14. Overall, qualitative and quantitative differences are observed. The 1*g* systems consistently exhibit higher cyclic moment capacity and accumulate more settlement than the
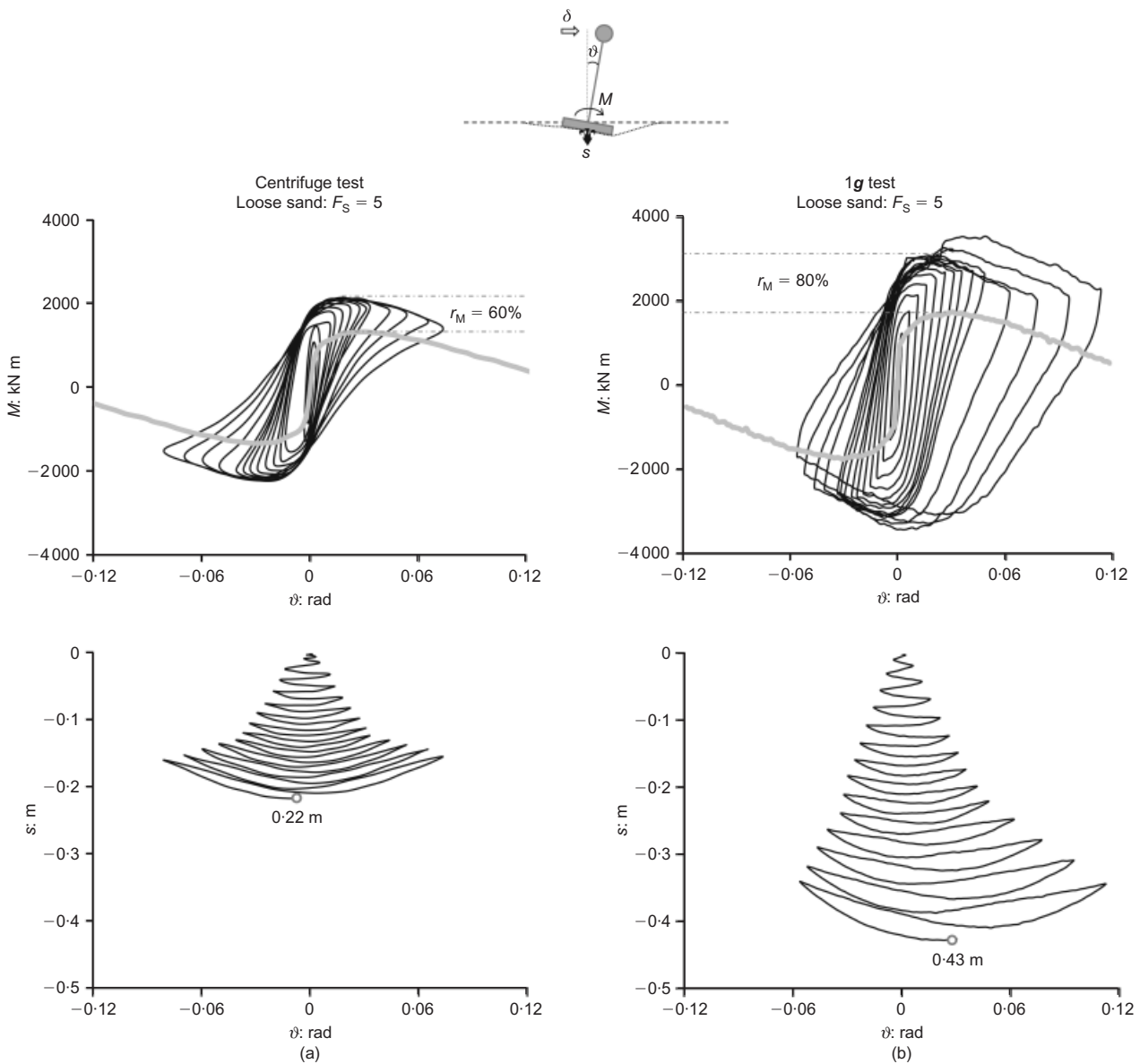

Fig. 12. Moment–rotation and settlement–rotation curves obtained from slow cyclic tests on loose sand ($D_r = 45\%$): (a) centrifuge test; (b) 1*g* test
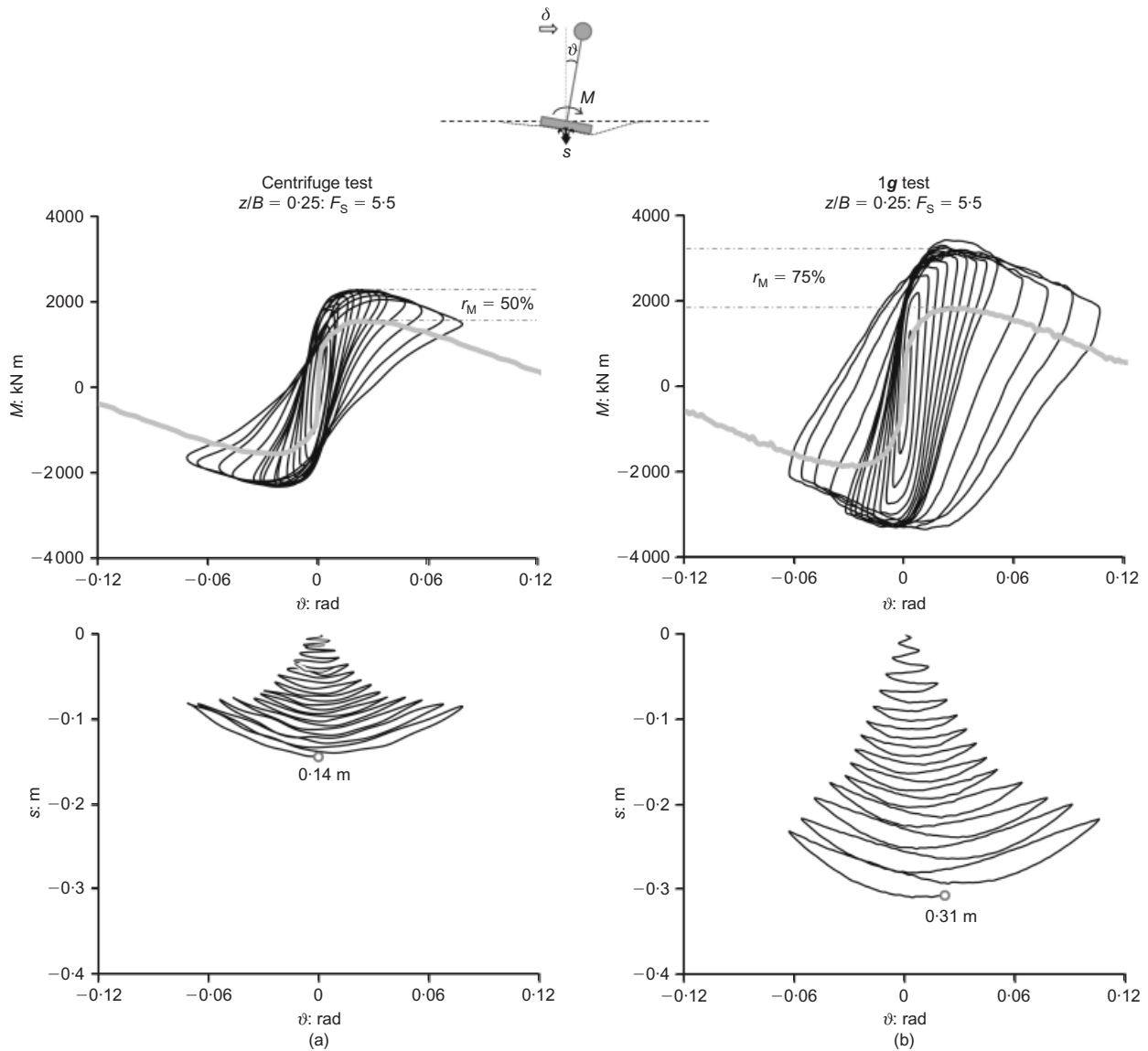
Fig. 13. Moment–rotation and settlement–rotation curves obtained from slow cyclic tests on two-layer soil profiles ($z/B = 0.25$): (a) centrifuge test, (b) 1g test

corresponding centrifuge systems. Nevertheless, the qualitative comparison reveals several interesting similarities between the response observed in the centrifuge and the 1g cyclic tests. The trend established in the monotonic pushover tests, where the moment capacity of the 1g tests reached higher levels, is also observed during cyclic loading. No substantial reduction of the moment capacity with number of cycles takes place. Additionally, a considerable amount of energy is dissipated in the foundation as suggested by the wide hysteresis loops. Rotational stiffness degradation is also observed and is discussed later in more detail.

The cyclic moment capacity well exceeds the monotonic backbone moment–rotation curve for all systems under comparison. This apparent moment overstrength can be quantified by an overstrength ratio r_M, defined as the increase in the cyclic moment capacity divided by the monotonic moment capacity. For the loosest soil and the 1g tests it reaches 80%; for the centrifuge tests it is smaller than 60%. In both types of test r_M is a function of the soil profile and the vertical factor of safety. Several interesting phenomena take place in parallel during cyclic loading: (a) densification of the soil under the footing, a phenomenon most prominent in

the loose sand tests but indicated by the decreasing rate of settlement accumulation in all settlement–rotation plots; (b) due to this compaction-style densification, the footing penetrates into the ground and hence it soon becomes essentially embedded; (c) on this denser soil layer the embedded footing enjoys a greater ultimate moment resistance, hence the great overstrength, especially for the 1g tests; (d) during large amplitude rotation angles ($\theta > 0.04$ rad), the footing (over an already denser soil) tends to uplift, although still eventually accumulates settlement. Similar trends have been noted by Drosos *et al.* (2012) and Anastasopoulos *et al.* (2013) in 1g experiments. But even for footings on saturated clay (under undrained conditions), Panagiotidou *et al.* (2012) observed theoretically a cyclic overstrength, which was attributed to the beneficial role of $P–\delta$ effects acting in the opposite to the loading direction. Hence, a portion of the observed overstrength is not necessarily related to densification.

The most evident difference between the centrifuge and the 1g tests lies in the accumulation of settlement during cyclic loading. The settlement response of the compared systems varies upon the vertical factor of safety. The systems on loose sand ($F_S = 5$) settle at the very first loading cycles of small
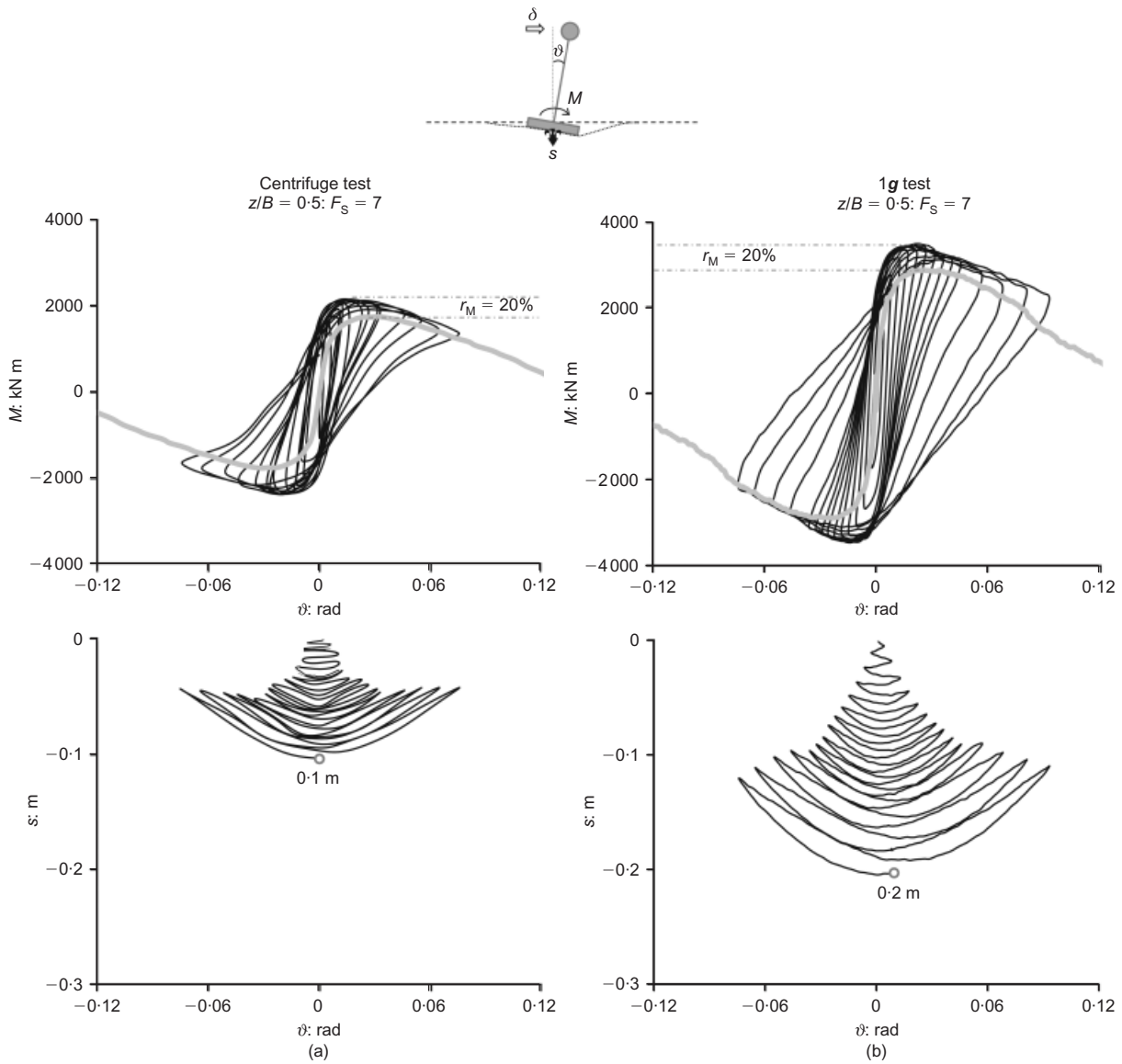
Fig. 14. Moment–rotation and settlement–rotation curves obtained from slow cyclic tests on two-layer soil profiles ($z/B = 0.5$): (a) centrifuge test; (b) 1g test

rotational amplitudes and tend to uplift while still accumulating settlement when larger displacement is applied. The systems on the two-layer profiles exhibit a more prominent uplifting behaviour, accumulating less settlement. This is particularly evident in the case of $z/B = 0.5$ ($F_S = 7$). For all soil profiles considered, the rate of settlement accumulation is larger in the 1g tests. At the end of the cyclic push test, the 1g systems have settled twice as much as the centrifuge systems. The settlement–rotation response is summarised in Fig. 15, plotting the settlement per cycle against the cycle rotation half-amplitude. The settlement is normalised to the foundation width B and the rotation is normalised to the overturning angle of the equivalent rigid block on rigid base ($\theta_R = B/2h$, where B is the block width and $2h$ is the block height). For all sets of systems ($F_S = 5$, 5.5 and 7) the settlement per cycle induced during the 1g slow cyclic push tests is higher at any rotational amplitude. The divergence becomes larger as the rotation increases and settlement obtained from the 1g tests reaches values up to double the settlement obtained from the centrifuge tests.

The cyclic settlement response contradicts the monotonic settlement response where the 1g systems exhibited more

pronounced uplifting behaviour. This could be attributed to the nature of cyclic loading and the potential for soil stiffening after multiple loading cycles. In an attempt to understand the cyclic settlement response, the last loading cycles of the cyclic loading tests on the $z/B = 0.5$ profiles are isolated and the settlement–rotation curves are compared in Fig. 16. The settlement accumulated in the previous cycles has been subtracted to allow more direct comparison. The two systems follow almost the same path in the first quarter cycle (A to B) up to the point that the centrifuge system enters the unloading quarter cycle, while the 1g system is still loaded to a slightly higher rotational amplitude. The difference in the response becomes clear during the unloading branch and continues thereafter. The accumulated settlement during this half cycle is larger for the 1g system. A reduced vertical stiffness of the 1g system that affects the unloading quarter cycle and the accumulation of settlement could be implied at this point. This hypothesis for the 1g system is further illustrated in the sketch of Fig. 16(b) (not drawn to scale). During the first quarter cycle (loading from A to B), large stress concentration takes place beneath the
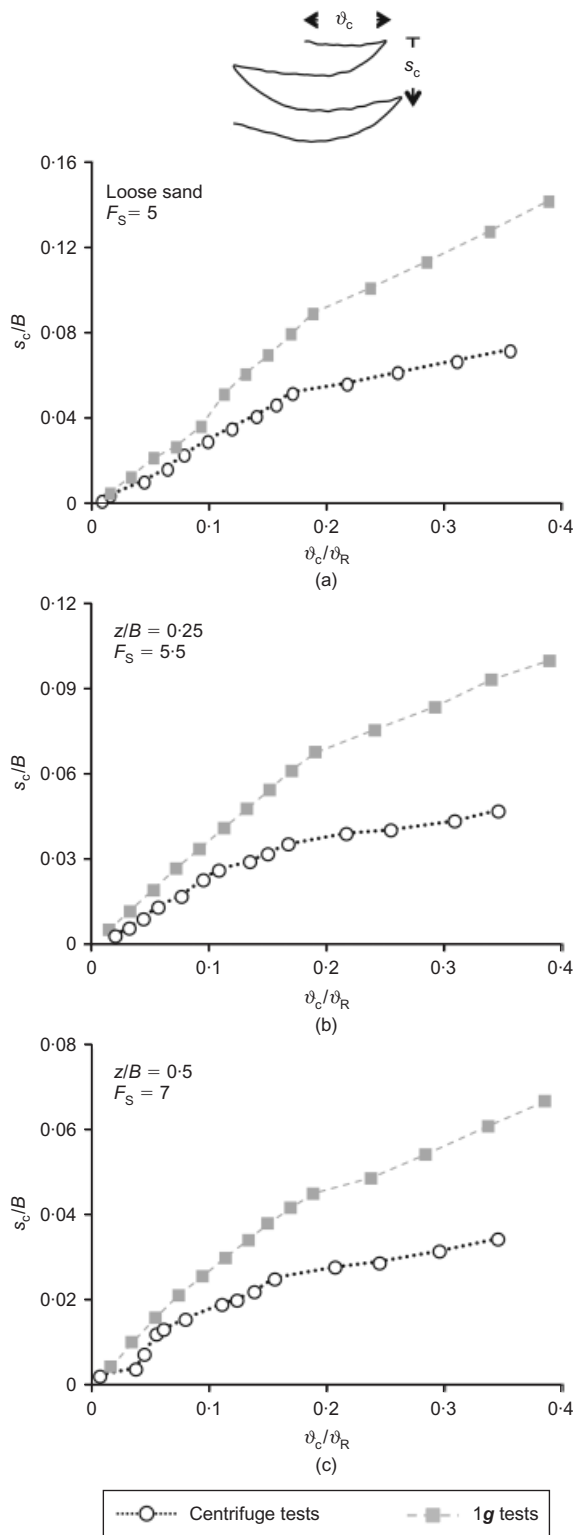
Fig. 15. Evolution of settlement during cyclic push tests: normalised settlement per cycle with respect to normalised cycle rotation half amplitude: (a) loose sand; (b) two-layer soil profile $z/B = 0.25$; (c) two-layer soil profile $z/B = 0.5$. B is the foundation width and θ_R is the overturning angle of the equivalent rigid block on rigid base

foundation corner as the latter uplifts from the supporting soil. As a result, at this stage scale effects are not important, as the geostatic stresses are not prevalent. As the second quarter cycle follows (unloading from B to C), the stress field under the uplifted footing becomes practically equal to

zero, and hence the geostatic stresses become prevalent and scale effects play a substantial role. And since the geostatic stresses are unrealistically low in the 1g tests, soil stiffness is much lower at this stage and until the foundation regains full contact with the soil, the potential for settlement is substantially larger. This phenomenon takes place in every unloading quarter cycle, leading to an overestimation of the settlement in the 1g tests.

Stiffness degradation and energy dissipation

As the systems are subjected to large amplitude rotation cycles, softening occurs and rotational stiffness degradation is observed. At these amplitudes a gap may form at one side of the footing while soil yielding occurs at the other side. In the following half cycle this phenomenon reverses and the gap has to close before the opposite corner of the footing starts uplifting. This gap formation and closing that occurs at large rotational amplitudes is responsible for the rotational stiffness degradation shown in the moment–rotation plots. The significant loss of contact between the foundation and the supporting soil results in reduction of the rotational stiffness of the unloading branches and produces the characteristic S-shape hysteresis loops. Even though the rotational stiffness degradation was evident in both centrifuge and 1g tests, the comparison with respect to the shape of the hysteresis loops reveals a fundamental difference: while the centrifuge tests produce distinct S-shaped loops, a more oval shape is demonstrated in the 1g plots. S-shaped moment–rotation response has been previously observed in centrifuge and large-scale experiments for systems with relatively high factor of safety or systems on dense soil (Gajan *et al.*, 2005; Negro *et al.*, 2000). In the same experimental investigations the moment–rotation curves were more oval-shaped for systems with lower factor of safety or systems on low-density sand.

This section explores the rotational stiffness degradation and energy dissipation that takes place during cyclic loading. To this end, the cyclic rotational stiffness and the damping ratio were calculated for the different loading cycles that the six systems were subjected to. Two different approaches were followed for these calculations and are illustrated in Fig. 17. According to method I, the rotational stiffness is defined as the slope of the line connecting the two tips of the moment–rotation loop. Since the maximum moment and maximum rotation do not occur simultaneously, an alternative rotational stiffness can be calculated as the ratio of the maximum moment to the maximum cycle rotation (method II). The respective elastic areas used for the calculation of the damping ratio are shown on this plot.

Figure 18 focuses on the rotational stiffness degradation and Fig. 19 on the dissipated energy during cyclic loading. In order to avoid misinterpretations due to inaccuracies in test measurements, the very first and small amplitude loading cycles are not included in the plots, and only cycles 3 to 14 are considered. The top graphs of Fig. 18 show the rotational stiffness as calculated according to the methods previously described. Following the trend noticed in the monotonic push tests, the rotational stiffness measured in the 1g tests is larger at any rotational amplitude. This agrees with the more oval shape of the 1g moment–rotation loops. In the bottom graphs the cyclic rotational stiffness is normalised to the small strain rotational stiffness as defined in the monotonic push over tests. Interestingly, the normalised results from the centrifuge and 1g tests follow identical degradation trend. In both absolute and normalised rotation plots, no distinct dependence of K_R on the soil profile (or alternatively the factor of safety) could be possibly extracted for the tests of the same type (centrifuge or 1g) since there
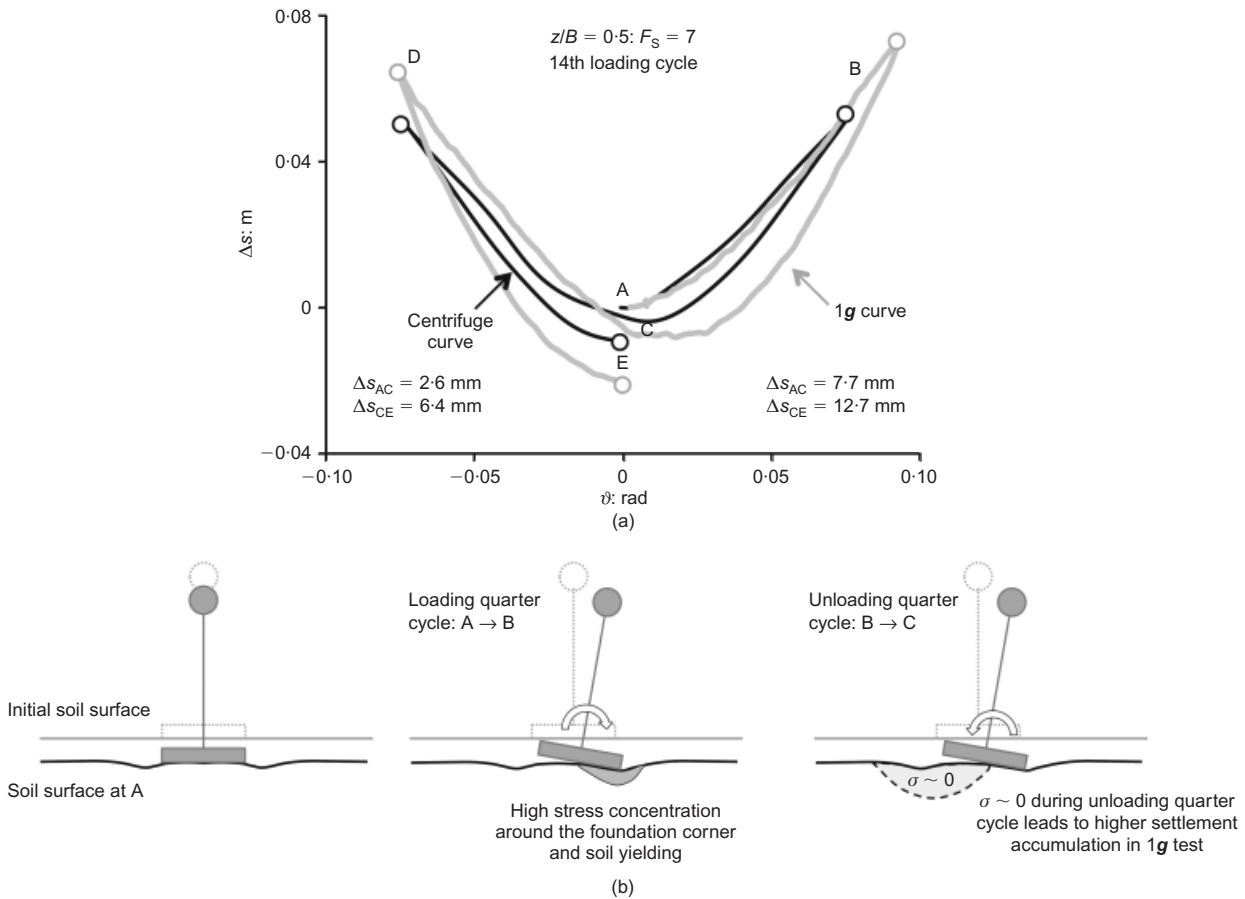
Fig. 16. (a) Settlement–rotation curve for the last loading cycle on the $z/B = 0.5$ profiles and comparison of settlement induced in each half cycle; (b) schematic illustration of the loading–unloading sequence in the 1g test (not drawn to scale)
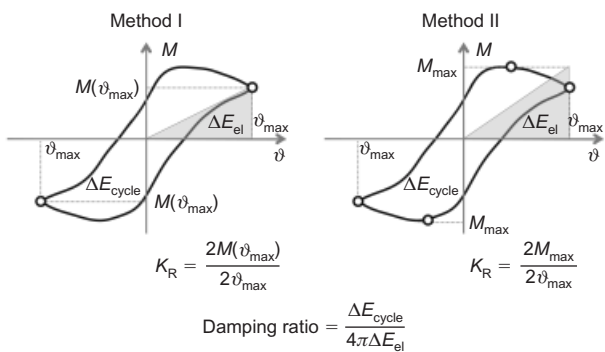

Fig. 17. Definition of cyclic rotational stiffness and damping ratio derived from the cyclic moment–rotation diagrams following two approaches

are no substantial differences in the rotational stiffness values of the loose and the two-layer profiles.

In the centrifuge tests, the damping ratio varies from 20% to 40%, being more or less independent of the soil conditions or, alternatively, of the F_S of the system. The damping ratio is slightly larger for small rotation amplitudes, but for $\theta > 0.03$ rad it remains constant. These observations apply to the results obtained by either method I or II. On the other hand, different trends are noted for the 1g tests. Increasing damping ratio with rotation is seen in the 1g tests that follow method I, while damping remains more or less constant when calculated with method II. In the first case the increase might be attributed to asymmetries in the cyclic loading that are also evident in the respective moment–

rotation plots. Additionally, some dependence on the soil conditions or the factor of safety is present. An increase of the damping ratio is noticed for decreasing factor of safety. Overall, the average damping values are slightly larger for the 1g tests.

SUMMARY AND CONCLUSIONS

An experimental study on dry sand was performed for the rocking response of slender systems, and for comparison between centrifuge and reduced-scale 1g tests. Equivalent (as much as possible) systems on three different soil profiles were subjected to monotonic and slow cyclic lateral loading. Before the lateral loading tests, the bearing capacity of the soil-foundation systems was measured through vertical push tests that provided additional information regarding the role of scale effects on bearing capacity. Based on the measured vertical ultimate force of each foundation, the systems were designed so as to maintain an analogy between the key dimensionless parameters of the rocking response: the vertical factor of safety F_S and the slenderness ratio h/B. The key conclusions can be summarised as follows.

- The low confining pressure prevailing in the 1g tests led to overestimation of the bearing capacity, since the effective friction angle of the soil is highly dependent on the stress level. This overestimation became more prominent when a dense sand profile was considered.
- The comparison between equivalent centrifuge and 1g lateral loading tests provided insight in several aspects of the problem. The 1g tests exhibited *qualitative*
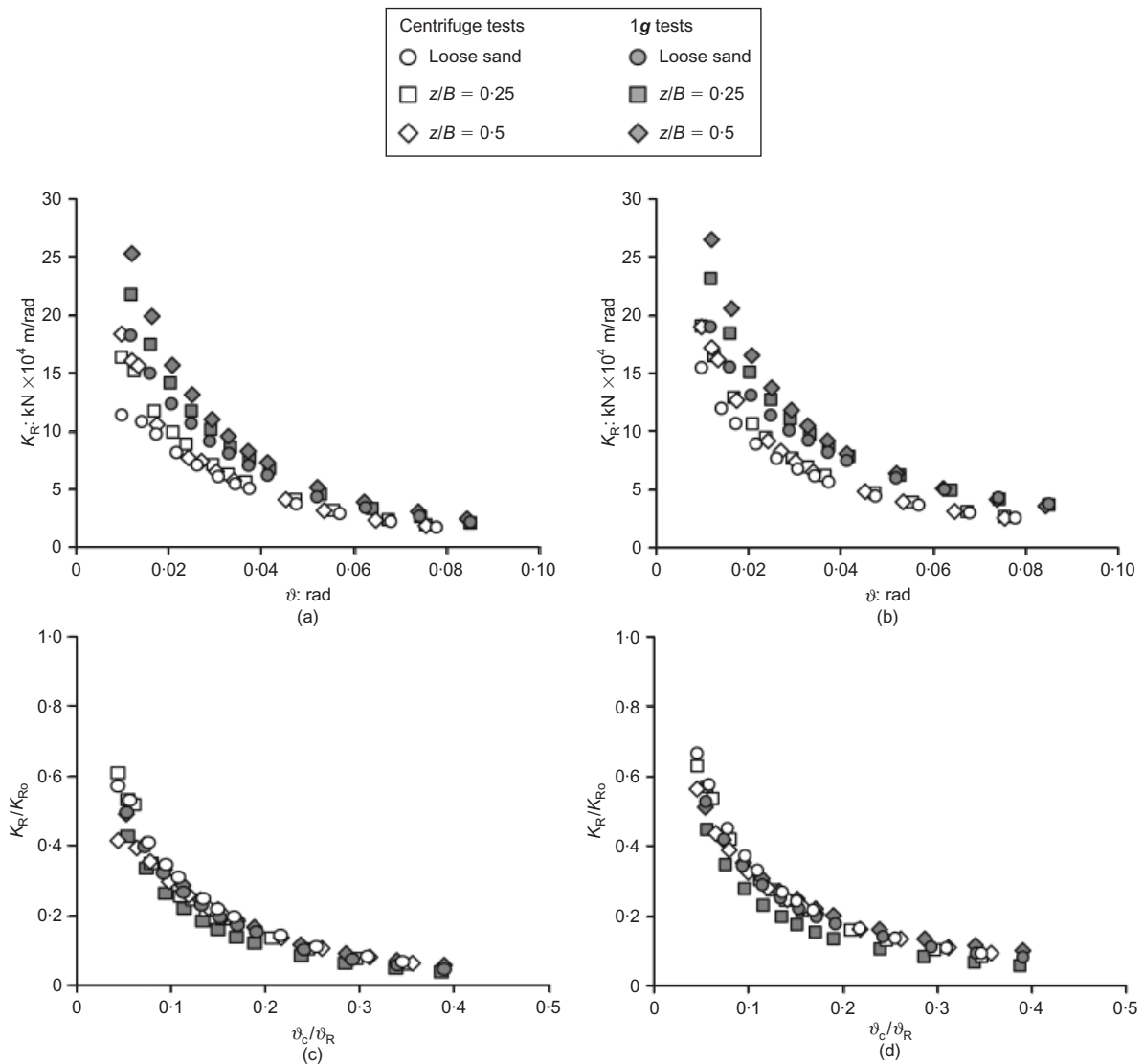
Fig. 18. Rotational stiffness degradation: top graphs show rotational stiffness plotted against cycle rotation half amplitude and bottom graphs show ratio of rotational stiffness K_R to small-strain rotational stiffness K_{Ro} as defined in the monotonic push tests plotted against the normalised cycle rotation half amplitude. The rotational stiffness was calculated according to method I in (a) and (c), and according to method II in (b) and (d)

similarities with the centrifuge tests capturing the highly ductile cyclic response, the stiffness degradation, the high level of energy dissipation of the rocking systems, as well as the cyclic moment overstrength. A difference was observed in the moment–rotation hysteresis loops, which were more oval-shaped in the 1g tests, offering larger energy dissipation.

- Densification of the sandy layers during cyclic loading clearly played a significant role in all the tests, either centrifuge or 1g.
- As expected, the quantitative comparison revealed discrepancies in terms of vertical and moment capacity as well as settlement accumulation. The increased moment capacity observed in the 1g tests is attributed to the overestimation of the angle of shearing resistance. The increased settlement is most probably due to the reduced vertical stiffness during the unloading phase of the loading sequence, when the effective stress exerted to the soil by the foundation is zero and the response is governed by the geostatic stresses.
- In terms of rotational stiffness degradation, the centrifuge and 1g systems showed the same normalised response

even though the actual rotational stiffness was larger in the 1g tests.

Summarising, the comparison presented in this paper showed that reduced-scale 1g tests can provide valuable insights to the rocking response of SDOF systems only if properly interpreted, with due consideration to the actual soil properties at very small confining pressures. This topic could be further explored with direct comparisons of true seismic shaking that could reveal potential differences related to the stress dependent dynamic soil behaviour and the characteristics of the applied ground motion. The experimental findings presented in this paper could serve as a baseline to interpret these differences.
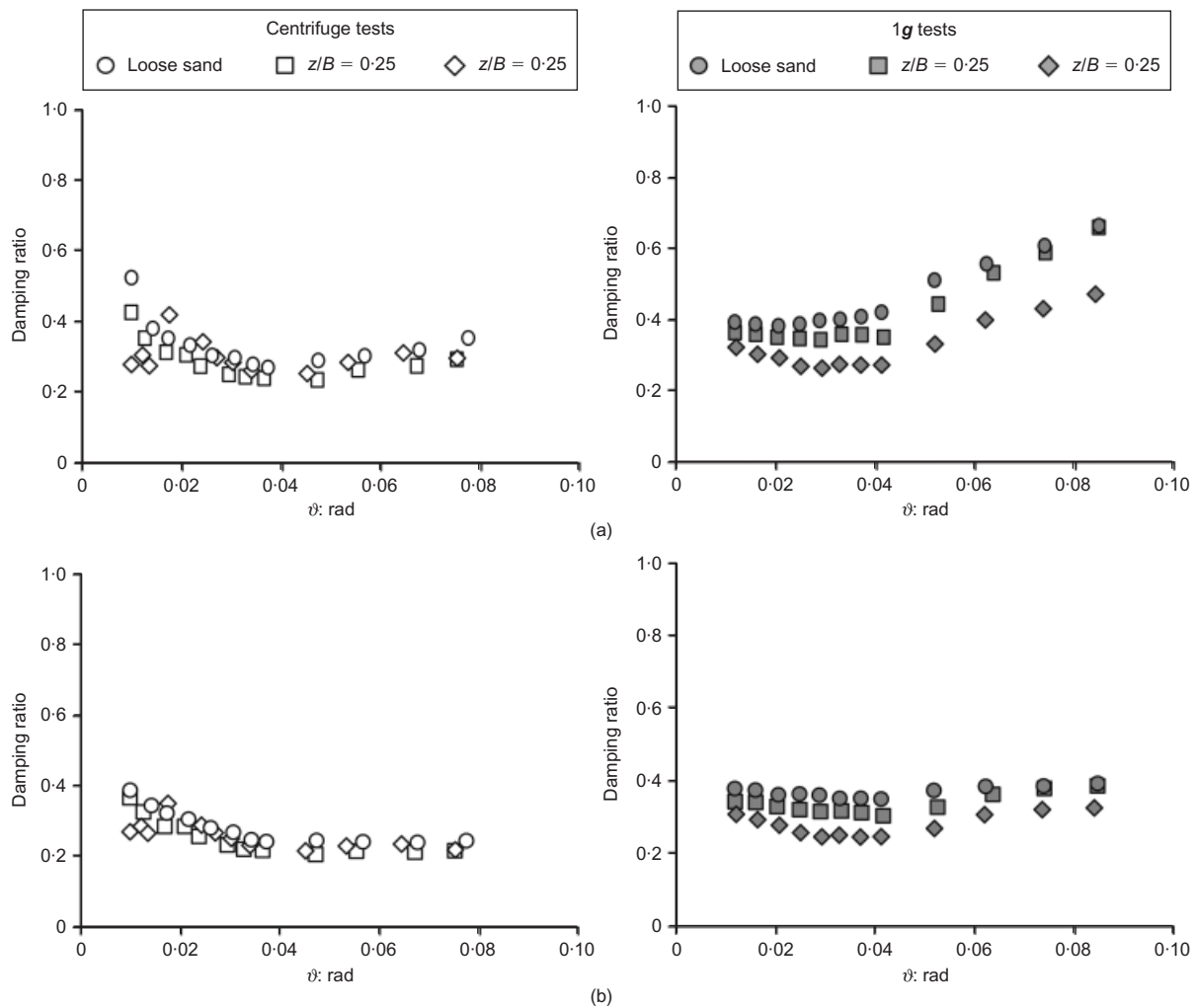
Fig. 19. Ratio of energy dissipation during cyclic push tests with respect to cycle rotation half amplitude. Damping was calculated according to method I in (a) and method II in (b)

REFERENCES

Anastasopoulos, I., Gazetas, G., Loli, M., Apostolou, M. N. & Gerolymos, N. (2010a). Soil failure can be used for seismic protection of structures. *Bull. Earthquake Engng* **8**, No. 2, 309–326.

Anastasopoulos, I., Georgarakos, P., Georgiannou, V., Drosos, V. & Kourkoulis, R. (2010b). Seismic performance of Bar-Mat reinforced-soil retaining wall: Shaking table testing versus numerical analysis with modified kinematic hardening constitutive model. *Soil Dynam. Earthquake Engng* **30**, No. 10, 1089–1105.

Anastasopoulos, I., Kourkoulis, R., Gelagoti, F. & Papadopoulos, E. (2012). Rocking response of SDOF systems on shallow improved sand: An experimental study. *Soil Dynam. Earthquake Engng* **40**, 15–33.

Anastasopoulos, I., Loli, M., Georgarakos, T. & Drosos, V. (2013). Shaking table testing of rocking-isolated bridge pier on sand. *J. Earthquake Engng* **17**, No. 1, 1–32.

Arulmoli, K., Muraleetharan, K. K. & Hossain, M. M. (1992). *VELACS –Verification of liquefaction analyses by centrifuge studies – Laboratory testing program*, Soil data report. Irvine, CA, USA: The Earth Technology Corporation.

Bransby, M. F. & Randolph, M. F. (1998). Combined loading of skirted foundations. *Géotechnique* **48**, No. 5, 637–655, http://dx.doi.org/10.1680/geot.1998.48.5.637.

Butterfield, R. & Gottardi, G. (1994). A complete three-dimensional failure envelope for shallow footings on sand. *Géotechnique* **44**, No. 1, 181–184, http://dx.doi.org/10.1680/geot.1994.44.1.181.

Chatzigogos, C. T., Pecker, A. & Salençon, J. (2009). Macroelement modeling of shallow foundations. *Soil Dynam. Earthquake Engng* **29**, No. 5, 765–781.

Deng, L., Kutter, B. L. & Kunnath, S. K. (2012). Centrifuge

modeling of bridge systems designed for rocking foundations. *J. Geotech. Geoenviron. Engng ASCE* **138**, No. 3, 335–344.

Drosos, V., Georgarakos, T., Loli, M., Anastasopoulos, I., Zarzouras, O. & Gazetas, G. (2012). Soil–foundation–structure interaction with mobilization of bearing capacity: An experimental study on sand. *J. Geotech. Geoenviron. Engng ASCE* **138**, No. 11, 1369–1386.

Gajan, S. & Kutter, B. L. (2008). Capacity, settlement and energy dissipation of shallow footings subjected to rocking. *J. Geotech. Geoenviron. Engng ASCE* **134**, No. 8, 1129–1141.

Gajan, S., Phalen, J. D., Kutter, B. L., Hutchinson, T. C. & Martin, G. (2005). Centrifuge modeling of load deformation behavior of rocking shallow foundations. *Soil Dynam. Earthquake Engng* **25**, No. 7–10, 773–783.

Gazetas, G. & Apostolou, M. (2004). Nonlinear soil–structure interaction: Foundation uplifting and soil yielding. In *Proceedings of the 3rd joint US–Japan workshop on soil–structure interaction*, Menlo Park, CA, pp. 60–66.

Gelagoti, F., Kourkoulis, R., Anastasopoulos, I. & Gazetas, G. (2012). Rocking isolation of low rise frame structures founded on separate footings. *Earthquake Engng Struct. Dynam.* **41**, No. 7, 1177–97.

Gourvenec, S. & Randolph, M. F. (2003). Effect of strength non-homogeneity on the shape and failure envelopes for combined loading of strip and circular foundations on clay. *Géotechnique* **53**, No. 6, 527–533, http://dx.doi.org/10.1680/geot.2003.53.6.575.

Kourkoulis, R., Anastasopoulos, I., Gelagoti, F. & Kokkali, P. (2012). Dimensional analysis of SDOF system rocking on inelastic soil. *J. Earthquake Engng* **16**, No. 7, 995–1022.

Martin, C. M. & Houlsby, G. T. (2001). Combined loading of

spudcan foundations on clay: numerical modelling. *Géotechnique* **51**, No. 8, 687–699, http://dx.doi.org/10.1680/geot.2001.51. 8.687.

Mergos, P. E. & Kawashima, K. (2005). Rocking isolation of a typical bridge pier on spread foundation. *J. Earthquake Engng* **9**, No. 2, 395–414.

Meyerhof, G. G. (1951). The ultimate bearing capacity of foundations. *Géotechnique* **2**, No. 4, 301–332, http://dx.doi.org/10. 1680/geot.1951.2.4.301.

Negro, P., Paolucci, R., Pedretti, S. & Faccioli, E. (2000). Large-scale soil–structure interaction experiments on sand under cyclic loading. In *Proceedings of the 12th world conference on earth-quake engineering*, Auckland, New Zealand, pp. 517–523. Upper Hutt, New Zealand: New Zealand National Society for Earthquake Engineering.

Nova, R. & Montrasio, L. (1991). Settlement of shallow foundations on sand. *Géotechnique* **41**, No. 2, 243–256, http://dx.doi.org/ 10.1680/geot.1991.41.2.243.

Panagiotidou, A. I., Gazetas, G. & Gerolymos, N. (2012). Pushover and seismic response of foundations on stiff clay: analysis with P–Delta effects. *Earthquake Spectra* **28**, No. 4, 1589–1618.

Paolucci, R. (1997). Simplified evaluation of earthquake induced permanent displacements of shallow foundations. *J. Earthquake Engng* **1**, No. 3, 563–579.

Paolucci, R., Shirato, M. & Yilmaz, M. T. (2008). Seismic behavior of shallow foundations: Shaking table experiments vs. numerical modeling. *Earthquake Engng Struct. Dynam.* **37**, No. 4, 577–595.

Pecker, A. & Pender, M. (2000). Earthquake resistant design of foundations: New construction. In *Proceedings of Geo-Engineering 2000 conference*, Melbourne, Australia, pp. 313–332.

Priestley, M. J. N., Seible, F. & Calvi, G. M. (1996). *Seismic design and retrofit of bridges*. New York, NY, USA: Wiley.

Wood, D. M. (2003). *Geotechnical modelling*. Boca Raton, FL, USA: CRC Press.